

Variations in the optical properties of terrigenous mineral-rich particulate matter suspended in seawater

Dariusz Stramski

Marine Physical Laboratory, Scripps Institution of Oceanography, University of California at San Diego, La Jolla, California 92093-0238

Marcel Babin

Laboratoire d'Océanographie de Villefranche, CNRS/Université Pierre et Marie Curie, B.P. 8, 06238 Villefranche-sur-Mer Cedex, France

Sławomir B. Woźniak

Institute of Oceanology, Polish Academy of Sciences, Powstańców Warszawy 55, 81-712 Sopot, Poland

Abstract

From laboratory measurements, we determined the spectral mass-specific absorption, $a_p^*(\lambda)$, and scattering, $b_p^*(\lambda)$, coefficients for terrigenous mineral-rich particulate assemblages suspended in seawater. The samples were derived mostly from surface soils in different locations and consisted of small particles ($<10 \mu\text{m}$). Both $a_p^*(\lambda)$ and $b_p^*(\lambda)$ showed large variability associated with variations in particle size distribution (PSD) and origin of samples. Variations in $a_p^*(\lambda)$ produced by changes in PSD are consistent with the package effect, in that samples with a higher percentage of small-sized particles have higher $a_p^*(\lambda)$. The variability among the samples is also associated with composition of particulate matter. For example, $a_p^*(\lambda)$ at blue wavelengths varied from $\sim 0.05 \text{ m}^2 \text{ g}^{-1}$ for organic-dominated soil dust to $\sim 0.1\text{--}0.5 \text{ m}^2 \text{ g}^{-1}$ for mineral-dominated samples. The effects of particulate composition are reflected in a broad range of imaginary refractive index of particles, which in the blue can exceed 0.2–0.3 for mineral-dominated samples rich in iron oxides. The patterns of the variability in the scattering coefficient among the samples are quite intricate because of the effects of PSD and composition. In general, $b_p^*(\lambda)$ ranged from about 0.5 to $1.5 \text{ m}^2 \text{ g}^{-1}$, and the spectral behavior varied from nearly flat spectra to the spectral dependency $\sim \lambda^{-\eta}$ with a slope η as high as ~ 1.3 for the sample with the largest contribution of small particles.

One of the greatest needs of ocean optics research is to improve knowledge and understanding of the absorption and scattering properties of suspended particulate matter at the level of detail that goes beyond the traditional description in terms of a few broadly defined bulk particulate categories, such as phytoplankton and non-phytoplankton (detrital) particles. Seawater is a complex optical medium and each of these broadly defined constituent categories includes in reality a great variety of particle types with different sizes, shapes, refractive indices, and, therefore, optical properties. Consequently, the same amounts of phytoplankton or nonphytoplankton particles parameterized in terms of bulk pigment concentration or bulk particle mass concentration in water can produce differences in the inherent optical properties (IOPs) characterizing absorption and scattering of light. This optical variability represents a major challenge that must be addressed by detailed studies of a comprehensive suite of properties of various particle types, such as different

plankton groups and species, different types of other biogenic particles, different mineral species and natural mixtures of mineral species, as well as mixed organic–inorganic particle types and assemblages.

The approach in which seawater is described as an optical medium consisting of a relatively large but manageable number of appropriately defined constituents should play a critical role in future efforts to advance the science of ocean optics and related applications, including ocean color remote sensing. This approach can be referred to as the reductionist approach. Previous studies discussed basic concepts underlying the reductionist approach and demonstrated, via initial examples, how powerful this approach can be (Mobley and Stramski 1997; Stramski and Mobley 1997; Stramski et al. 2001). One general conclusion that has emerged from these studies is that unless we move beyond a traditional paradigm of using just a few bulk particle categories, further advances in mechanistic understanding of optical variability in aquatic environments will be very difficult, if not impossible, to achieve (Stramski et al. 2004a). In this study, which is largely motivated by our goal to make progress in this direction, our interest is focused on the poorly investigated portion of nonliving marine particulate matter that is not derived from marine plankton organisms and biological processes, such as grazing, viral infection, and natural mortality. We examine terrigenous mineral-rich assemblages of particles suspended in seawater, consisting essentially of small particles ($<10 \mu\text{m}$ in size)

Acknowledgments

The analysis of samples for particulate organic carbon was made at Marine Science Institute Analytical Laboratory, University of California at Santa Barbara. We thank A. Wiedemann and an anonymous reviewer for comments on the manuscript. This study was supported by National Aeronautics and Space Administration (NNG04GK50G) and Office of Naval Research (N00014-98-1-0003).

derived primarily from surface soils. These small particles have the potential for relatively long residence times in the upper water column (Lerman et al. 1977), and their presence in marine environments results from terrestrial runoff, coastal erosion, and deposition of atmospheric dust (e.g., Carder et al. 1986; Beusen et al. 2005). We note that there can also be anthropogenic contributions to this category of particulate assemblages.

Recent laboratory measurements revealed significant variability in the spectral mass-specific absorption coefficient, $a_p^*(\lambda)$, and scattering coefficient, $b_p^*(\lambda)$ (where λ denotes light wavelength in a vacuum), of mineral-rich particulate assemblages suspended in water (Babin and Stramski 2004; Stramski et al. 2004b). The variability in $a_p^*(\lambda)$ and $b_p^*(\lambda)$ was also demonstrated in field experiments conducted in mineral-rich coastal waters (e.g., Babin et al. 2003a,b; Bowers and Binding 2006). Both laboratory and field studies have strengths and weaknesses and play complementary roles in research on particle optics. Typically, carefully designed laboratory studies offer an advantage of quite accurate methods and a broad range of measurements that might not be possible during field experiments. Although this approach facilitates the development of a mechanistic understanding of sources of variability in particle optical properties, the particulate assemblages studied in the laboratory might not always represent well enough the properties of particles in situ. In field studies, various measurements can be made in situ but the assortment of measured variables and accuracy of the methodology are generally more limiting than in laboratory. Also, achieving a detailed understanding of the sources of optical variability is quite difficult with field measurements alone.

The samples examined in laboratory studies of Babin and Stramski (2004) and Stramski et al. (2004b) originated from different locations on Earth and differed from one another in terms of mineralogical and elemental composition. Babin and Stramski (2004) showed that a significant part of the observed variation in $a_p^*(\lambda)$, especially in the ultraviolet, blue, and green spectral regions, can be attributed to changes in the iron content of mineral particles. This result is consistent with earlier observations that iron is a major pigmentation agent in mineral-dominated soils, sediments, and atmospheric dust (Torrent et al. 1983; Deaton and Balsam 1991; Arimoto et al. 2002). Another source of variability in $a_p^*(\lambda)$ is associated with particle size distribution (PSD), but this problem was not addressed in earlier experiments. In general, if the mineralogical and chemical composition of a given particulate assemblage remains unchanged, $a_p^*(\lambda)$ is expected to decrease with a decrease in the proportion of small-sized particles. This effect was shown in a theoretical study of the optical properties of mineral particles suspended in water with a model of homogeneous spherical particles (Woźniak and Stramski 2004). Theoretical studies also show that variations in PSD and refractive index of mineral particles are the first-order determinants of variability in the mass-specific scattering coefficient, $b_p^*(\lambda)$ (Babin et al. 2003a; Woźniak and Stramski 2004). So far, however, few experiments under controlled laboratory conditions have

been conducted to quantify the variability in $b_p^*(\lambda)$ for mineral-dominated particulate assemblages suspended in seawater (Stramski et al. 2004b).

In addition to the effects of PSD, $a_p^*(\lambda)$ depends on the imaginary part of the refractive index, $n'(\lambda)$, of particles. The $n'(\lambda)$ values are related directly to the absorption coefficient of matter forming the particle, $a_{pm}(\lambda)$, and hence the intraparticle concentration of absorbing substances (e.g., Morel and Bricaud 1981). For marine phytoplankton cells, for example, n' in the spectral region near 670 nm was shown to correlate well with the intracellular concentration of chlorophyll *a* (Chl *a*), a major pigment that absorbs light in that red waveband (Stramski 1999). Although $n'(\lambda)$, or equivalently $a_{pm}(\lambda)$, is a key property of particles that characterizes their capacity to absorb light, to our knowledge the determinations of $n'(\lambda)$ for mineral-rich natural assemblages of particles suspended in water have not been attempted in the past.

Because theoretical studies of marine particles are naturally based on simplified assumptions about particle properties such as size distribution, refractive index, and shape, it is very useful to make measurements on actual particle suspensions. In this study, we report on laboratory determinations of $a_p^*(\lambda)$ and $b_p^*(\lambda)$ for various samples of mineral-rich particulate matter suspended in seawater. Our primary objective is to show how an alteration of PSD resulting from selective removal of particles by settling from a given particulate assemblage influences light absorption and scattering by this assemblage. We demonstrate these effects for a number of particulate assemblages of different origins, including assemblages composed of essentially one mineral species, as well as mineral-rich mixed assemblages that comprise several mineral species in significant amounts and variable contribution of organic matter. Our experiments also provide insight into variations in the imaginary refractive index of the particulate assemblages.

The effects of PSD and $n'(\lambda)$ on absorption can be interpreted in terms of the so-called package effect (Duysens 1956; Morel and Bricaud 1981). For marine algal cells, it has been recognized that variations in the Chl *a*-specific absorption coefficient are driven partly by the package effect (Morel and Bricaud 1981). It was shown that the package effect results in a decrease of Chl *a*-specific absorption of phytoplankton in response to an increase in cell size, an increase in n' (i.e., an increase in intracellular pigment concentration), or both. In this study, we provide experimental evidence that an analogous phenomenon of package effect is pertinent to the mass-specific absorption coefficient of mineral-rich assemblages of real (i.e., generally nonspherical and internally heterogeneous) particles suspended in water.

Materials and methods

Description of samples—Two groups of samples were examined: first, the particulate assemblages composed of essentially one mineral species and, second, the mineral-rich particulate assemblages comprising several mineral species in significant amounts (Table 1). The first group

Table 1. Description and origin of particle samples analyzed in this study. For most samples, the measurements were made with two different particle size distributions, indicated with subscripts “1” and “2” in the sample identifier (ID). The values for the concentration of suspended particulate matter (SPM) are given. For some samples, the particulate organic carbon (POC) concentration is also given.

ID	Description	Origin	SPM (g m ⁻³)	POC (g m ⁻³)
ILL ₁	Illite	Source Clay Minerals Repository, University of Missouri (ref. IMt-1)	37.71	
ILL ₂	As above but different PSD	As above	26.53	0.86
KAO ₁	Kaolinite (poorly crystallized)	As above, but ref. KGa-2	28.34	
KAO ₂	As above but different PSD	As above	23.3	
MON ₁	Ca-montmorillonite	As above, but ref. SAz-1	38.48	
MON ₂	As above but different PSD	As above	28.52	0.73
CAL ₁	Calcite	Natural crystal	26.48	
CAL ₂	As above but different PSD	As above	12.60	
QUA ₁	Quartz	Natural crystal	14.17	
SAH ₁	Atmospheric dust from Sahara	Red rain event, Villefranche-sur-Mer, France, Nov 1996	43.43	1.28
SAH ₂	As above but different PSD	As above	19.47	
AUS ₁	Surface soil dust	Cliff shore, Palm Beach north of Sydney, Australia	32.03	0.87
AUS ₂	As above but different PSD	As above	24.05	0.64
ICE ₁	Ice-rafted particles	Glacier runoff, Kongsfjord, Spitsbergen, Norway	28.51	0.44
ICE ₂	As above but different PSD	As above	22.37	
OAH ₁	Surface soil dust	Oahu, Hawaii Islands	31.67	1.12
OAH ₂	As above but different PSD	As above	18.05	0.62
KUW ₁	Surface soil dust	Kuwait (eastern part, close to ocean)	23.36	
KUW ₂	As above but different PSD	As above	23.10	6.27
NIG ₁	Surface soil dust	Southwest Nigeria	37.06	2.71
SAN ₁	Atmospheric dust	San Diego, California	17.08	2.73

included illite (ILL), kaolinite (KAO), montmorillonite (MON), calcite (CAL), and quartz (QUA). The second group included natural samples of various origins such as atmospheric dust from the Sahara (SAH) and from southern California (SAN), ice-rafted particles from the polar environment of Spitsbergen, Norway (ICE), and surface soil dust from several locations on Earth (AUS, Australia; OAH, Oahu Island, Hawaii; KUW, Kuwait; NIG, Nigeria). For convenience, this second group will be referred to as “mixed samples” or “mixed particulate assemblages.” The range of samples and terrestrial environments from which they originate entail soil particles that can be delivered to marine environments via different mechanisms, such as atmospheric deposition, melting of coastal glaciers, shore erosion, and terrestrial runoff. An important aspect of our experiments is that, for most samples, the measurements were made for two different PSDs. This is indicated with subscripts “1” and “2” that accompany the sample identifiers (*see* Table 1). More details on the origin and collection of all samples with the exception of OAH and SAN can be found in Babin and Stramski (2004). The OAH sample is the surface soil dust of reddish appearance, which was collected on Oahu

Island. The SAN sample is the atmospheric dust that was collected by wet deposition during a weak rain event in San Diego near the end of a Santa Ana event, which is characterized by dry and warm, often hot and dusty, northeasterly winds in southwestern California that occur mostly during fall, winter, and spring (Raphael 2003). Significant amounts of airborne dust are usually blown out of the desert toward the coastal areas with Santa Ana winds.

Before measurements were taken, a powder sample of particles was suspended in filtered seawater (0.2- μ m Nalgene syringe filter after prefiltration with Whatman GF/F filter) to produce an initial particle suspension of a given sample. Seawater was taken at the pier of the Scripps Institution of Oceanography. For most samples (with the exception of QUA, NIG, and SAN), two final particle suspensions were prepared from the initial suspension with the purpose of producing two different PSDs. The first sample (sample identified with subscript “1”) was obtained by allowing particles in the initial suspension (200–600 mL, depending on the sample) to settle gravitationally for \sim 25 min in a 1-L beaker. This sedimentation removed a fraction of relatively large particles from the

suspension. After the sedimentation period, the particle suspension was first separated from the fraction remaining at and near the bottom of the sedimentation beaker, and it was then exposed to ultrasonication for a few minutes. This final suspension was used for optical measurements and other analyses. The second sample (subscript “2”) was prepared in a similar way, but with a longer sedimentation period in an Andreasen pipette (Allen 1981), ranging from about 2 to 5 h, depending on the sample. Because of the longer sedimentation period, sample 2 was characterized by a higher proportion of small-sized particles compared with sample 1. We note that all powder samples with the exception of OAH and SAN have been used in our previous study (Babin and Stramski 2004), which focused on examining the absorption spectra but did not include the PSD measurements and determinations of scattering spectra. We also note that in contrast to all other samples examined in this study, SAN and KUW are characterized by relatively high organic particle content. Therefore, this study includes samples dominated by mineral particles as well as a few samples in which both organic and inorganic particle types are important.

PSD, dry weight, and POC analysis—PSD was measured between the equivalent spherical diameters D of 0.85 and 18 μm with a Beckman-Coulter Multisizer III equipped with a 30- μm aperture tube. The data for $D < 0.85 \mu\text{m}$ were omitted from our analysis to avoid the effects of instrument noise at the lower limit of detection. To minimize coincidence effects, the particle counts were made on sufficiently dilute suspensions (i.e., diluted four times compared with samples used in optical measurements). Nevertheless, the coincidence correction was applied when the raw PSD data were processed with Beckman-Coulter software (Coulter AccuComp ver. 3.01a). The final PSDs were calculated by averaging three replicate measurements, each usually made on 0.1 mL of the sample (occasionally 0.05 or 0.2 mL) and subtracting an average blank measurement made on filtered seawater. The dilution was accounted for in these final calculations. Because the optical measurements of the beam attenuation and absorption coefficients (*see* description below) were separated in time (albeit never more than 1 h), the PSD measurements were made twice; first, during the attenuation measurement and then again during the absorption measurements. We observed no significant changes in PSD within the time period necessary to complete the optical measurements. We present PSDs obtained by averaging measurements taken during the attenuation and absorption measurements.

In parallel to the optical and PSD measurements, 30 mL of sample (20 mL on a few occasions) were filtered onto preweighed 0.2- μm Cyclopore polycarbonate membrane filters (Whatman). At the end of filtration, deionized water was passed through the filters to wash out a residual amount of sea salt. The filters were then dried at room temperature at relative humidity of 30–40% for a few days before measuring the mass of particles with a micrometric balance (MT5, Mettler-Toledo). The dry mass concentration of suspended particulate matter (SPM) per unit

volume of water (g m^{-3}) for each sample was determined from weight measurements on three replicate filters. The coefficient of variation for the replicates was $<5\%$ (for most samples $<3\%$). For comparative purposes, we also tested the determination of SPM on 0.2- μm Nuclepore polycarbonate membrane filters (Whatman) and 0.02- μm Anopore aluminum oxide membrane filters (Anodisc, Whatman). These tests showed very good agreement (i.e., on average to within 1%) between the 0.2- μm Cyclopore and Nuclepore filters. This agreement is not surprising because both filter types are track-etched polycarbonate membranes with sharply defined pore sizes manufactured in a similar fashion. The SPM values determined with 0.02- μm Anopore filters were usually also similar to those obtained with 0.2- μm filters. However, for a few samples, the difference between the determinations on the 0.02- and the 0.2- μm filters exceeded 30% (both + and –). In this study we use the SPM values determined with the 0.2- μm Cyclopore filters. We note that different names and symbols are used in oceanographic literature to indicate the measurement of SPM, for example, total suspended matter (TSM) or total suspended solid (TSS). We prefer to use SPM because, in principle, not all particles are included in this measurement.

The concentration of particulate organic carbon (POC) was determined by means of high-temperature combustion (1,000°C) with a CEC 440HA elemental analyzer (Control Equipment Corp., now Exeter Analytical). For these determinations, the samples were prepared by filtering 30 mL of the particle suspension onto GF/F filters (Whatman) precombusted at 450°C for 1 h. At the end of filtration, sea salt was rinsed off the filters with deionized water. The filters were then dried at 55°C and stored until carbon analysis. Before the analysis, the filters were treated with 0.25 mL of 10% HCl to remove inorganic carbon. The final POC concentrations were calculated from the mass of organic carbon measured on the sample filter and from the volume of sample filtered. In these calculations, the correction was made for the average mass of carbon determined for blank filters. Although the POC determinations do not provide exact information on the total particulate organic matter, they offer a means for comparing the samples in terms of approximate contribution of organic matter to SPM.

Optical measurements—Optical measurements of the absorption coefficient of particles, $a_p(\lambda)$, and the beam attenuation coefficient of particles, $c_p(\lambda)$, were made in a spectral region from 300 to 850 nm at 1-nm intervals with a dual-beam spectrophotometer (Lambda 18, Perkin Elmer) equipped with a 15-cm Spectralon integrating sphere (RSA-PE-18, Labsphere). The methods of these measurements are described in detail in our previous studies (Babin and Stramski 2004; Stramski et al. 2004b). Here, we summarize some important aspects of this methodology.

For measuring $c_p(\lambda)$, the sample of particle suspension in 1-cm quartz cuvette was placed at a significant distance from the detector (~ 25 cm from the entrance port to the integrating sphere), and field stops were aligned within the light path to

reduce the size of the beam and acceptance angle of the detector to less than 1° . The baseline spectrum representing the “particle-free” reference was measured on 0.2- μm filtered seawater. The sample measurements were made on optically thin particle suspensions with $c_p < 40 \text{ m}^{-1}$ ($< 30 \text{ m}^{-1}$ for $\lambda > 400 \text{ nm}$). These conditions ensured high enough optical signal while maintaining the effects of multiple scattering in a 1-cm cuvette at a practically undetectable level (Bricaud et al. 1988; Stramski and Piskozub 2003). The $c_p(\lambda)$ measurement was always made first before $a_p(\lambda)$ and other measurements (PSD, SPM, and POC), which allowed us to prepare the final sample for all analyses with an appropriate optical thickness by dilution with particle-free seawater (i.e., 0.2- μm filtrate). The values of $c_p(\lambda)$ (m^{-1}) were calculated by multiplying the measurements of the baseline-corrected optical density OD (i.e., absorbance measured with a spectrophotometer in the beam attenuation setup) of the sample by $\ln(10)$ and dividing by the path length ($=0.01 \text{ m}$).

The absorption measurements were made on samples of particle suspension in a 1-cm cuvette that was placed inside the integrating sphere so that the incoming incident beam was normally incident on the cuvette wall. For the baseline measurement, the cuvette filled with filtered seawater was used. The most significant advantage of this geometry is that the measurement of particle absorption is subject to only a small scattering error (Haardt and Maske 1987; Babin and Stramski 2002). However, small artifacts can still be observed, in particular a small negative offset in the measured absorbance values when true absorption of particles is null or very weak, which often happens in the far red and near infrared (near-IR, $\sim 700\text{--}850 \text{ nm}$) spectral region. The difference between the scattering sample and particle-free reference in terms of light reflected by cuvette walls and escaping from the integrating sphere was suggested as a primary source for this offset (Babin and Stramski 2002; Tassan and Ferrari 2003). We note that for other instrumentation and measurement geometries that have been commonly used to measure absorption of aquatic particles, the offset because of scattering error is typically positive and significantly larger than in our present measurement system (e.g., Bricaud et al. 1983; Zaneveld et al. 1994; Stramski and Piskozub 2003).

A simple way of correcting for these artifacts would be to shift the measured spectrum by a value corresponding to the offset in the near-IR region, so the resulting absorption values at these wavelengths are zero. This type of correction is often referred to as null-point correction, which in effect assumes no particle absorption in the near-IR. The drawback of this correction is that certain particle types or assemblages could exhibit absorption in the near-IR (e.g., Tassan and Ferrari 2003; Babin and Stramski 2004; Bowers and Binding 2006). However, this absorption signal is usually weak and difficult to quantify accurately. Although most of our previously reported results for mineral-dominated samples have the limitation associated with the use of null-point correction, we also made special experiments that showed sizable absorption in the near-IR for some samples (Babin and Stramski 2004; Stramski et al. 2004b).

In this study we have not applied the null-point correction; instead, we used the following approach for correction. The absorption by calcite particles within the examined range of visible and near-IR wavelengths is so low (Lindberg 1975; Sokolik and Toon 1999) that it can be assumed negligible for our purposes. For the calcite samples, CAL₁ and CAL₂, we calculated the parameter $\alpha(\lambda) = \text{OD}_a(\lambda)/\text{OD}_c(\lambda)$, where the optical densities OD_a and OD_c are baseline-corrected. The subscript “a” indicates that the measurement was made in the absorption setup of the spectrophotometer, and the subscript “c” indicates the beam attenuation setup. If true absorption at λ is zero, which for our practical purposes is a reasonable assumption for calcite, then $\alpha(\lambda)$ is the fraction of scattering that is being measured in the absorption setup.

For both CAL₁ and CAL₂, $\alpha(\lambda)$ was weakly dependent on λ and assumed values close to -0.05 within the wavelength range 700–800 nm. The negative sign of $\alpha(\lambda)$ indicates a negative offset in the absorption signal because of scattering/reflection effects (see Babin and Stramski 2002). The absorption measurements for all samples examined in this study were corrected for this error according to Eq. 1

$$a_p(\lambda) = \frac{a'_p(\lambda) - \alpha c_p(\lambda)}{1 - \alpha} \quad (1)$$

where $a_p(\lambda)$ is the final corrected absorption coefficient of particles (m^{-1}), $a'_p(\lambda)$ is the measured (uncorrected) absorption coefficient of particles, $c_p(\lambda)$ is the measured beam attenuation coefficient of particles, and α is assumed to be -0.05 for all wavelengths. The uncorrected coefficient $a'_p(\lambda)$ was calculated by multiplying the measurements of the baseline-corrected OD of the sample (obtained in the absorption setup) by $\ln(10)$ and dividing by the path length ($=0.01 \text{ m}$). Note that in principle, α could have also been determined from measurements of the QUA₁ sample because quartz also shows negligible absorption within the examined spectral range (Peterson and Weinman 1969; Lindberg 1975; Sokolik and Toon 1999). However, we have chosen to use calcite-based α because the $c_p(\lambda)$ values for CAL₁ and CAL₂ ranged from about 13 m^{-1} to over 30 m^{-1} , which is consistent with the range of $c_p(\lambda)$ for all other samples examined in this study. In contrast, the QUA₁ sample had lower $c_p(\lambda)$ of $\sim 10\text{--}13 \text{ m}^{-1}$.

The final results of $a_p(\lambda)$ and $c_p(\lambda)$ were calculated by averaging duplicate or triplicate spectral scans made on samples and particle-free reference. The spectral scattering coefficient of particles, $b_p(\lambda)$, was calculated as the difference $c_p(\lambda) - a_p(\lambda)$. The mass-specific absorption coefficient, $a_p^*(\lambda)$, and the mass-specific scattering coefficient, $b_p^*(\lambda)$ ($\text{m}^2 \text{ g}^{-1}$), of particulate matter were calculated as the ratio of the absorption, $a_p(\lambda)$, and scattering, $b_p(\lambda)$, coefficients of particles, respectively, to the mass concentration of particles, SPM. We also calculated the POC-specific coefficients by normalizing $a_p(\lambda)$ and $b_p(\lambda)$ to the POC concentration.

Imaginary part of refractive index—The method for estimating the imaginary part of the refractive index of phytoplankton, $n''(\lambda)$, on the basis of measurements of

absorption, beam attenuation, and PSD, was described in Bricaud and Morel (1986). This method cannot be used in our study because it is highly sensitive to the accuracy of the measurement of the total number concentration of absorbing particles in the sample (for the same reason, the application of an inverse optical method for estimating the real refractive index from our data is impossible). In our experiments, significant contribution to this total number concentration comes from small particles below the limit of detection of our Beckman-Coulter instrument for particle counting. Therefore, we have taken another approach to estimate $n'(\lambda)$. We start with an assumption that the optical property of the bulk medium can be related to the optical properties of the medium constituents and their respective volume fractions. On assuming that the mixture of two constituents, pure water and particles immersed in water, behaves as an effective medium that satisfies the Biot-Arago mixing rule with volume additivity, we can write the bulk absorption coefficient of the mixture as (e.g., Lindberg et al. 1999)

$$a(\lambda) = a_{\text{pm}}(\lambda) \frac{V_p}{V} + a_w(\lambda) \frac{V_w}{V} \quad (2)$$

where $a_{\text{pm}}(\lambda)$ is the absorption coefficient of matter forming the particles, $a_w(\lambda)$ is the absorption coefficient of pure water, V_p and V_w are the volumes occupied by particles and water, respectively, and $V = V_p + V_w$. We will denote the volume fractions as $V'_p = V_p/V$ and $V'_w = V_w/V$. The coefficient $a_{\text{pm}}(\lambda)$ is an intrinsic property of a particulate material related to imaginary refractive index and should not be confused with the absorption coefficient of particles in suspension, $a_p(\lambda)$.

We used Eq. 2 in combination with our absorption and particle size measurements to derive approximate values for the lower limit of imaginary refractive index of particles in the following way. Equation 2 can be viewed as an expression of our spectrophotometric measurement of absorption of the sample when the cuvette contains particles suspended in water. To determine the particulate absorption coefficient, $a_p(\lambda)$, the measurement made on filtered seawater (i.e., baseline) must be subtracted from the sample measurement. Therefore, on subtracting the pure water absorption coefficient, $a_w(\lambda)$, from both sides of Eq. 2 and rearranging, we obtain

$$a_{\text{pm}}(\lambda) = \frac{a_p(\lambda) + a_w(\lambda)[1 - V'_w]}{V'_p} = \frac{a_p(\lambda)}{V'_p} + a_w(\lambda) \quad (3)$$

given that $V'_p + V'_w = 1$. We calculated $a_{\text{pm}}(\lambda)$ with the $a_p(\lambda)$ from our spectrophotometric measurements (see Eq. 1). The $a_w(\lambda)$ data over the spectral range examined were taken from several studies (Hale and Querry 1973; Smith and Baker 1981; Pope and Fry 1997; Sogandares and Fry 1997). The volume fraction of particles, V'_p , was calculated by integrating the measured size distributions expressed in terms of particle volume concentration, $F_V(D)$. The integration over the range of measured particle sizes ($D = 0.85\text{--}18 \mu\text{m}$) would underestimate the actual V'_p , primarily because of the missing contribution of small particles $<0.85 \mu\text{m}$. Therefore, to calculate V'_p , we made a linear extrapolation of $F_V(D)$ to zero at $D = 0.01 \mu\text{m}$. The

upper limit of integration was $18 \mu\text{m}$, but the contribution of sizes of $>10 \mu\text{m}$ to V'_p was very small.

The estimation of total V'_p that includes the extrapolation for $D < 0.85 \mu\text{m}$ is more reliable for samples 1 than for those from samples 2. This is because the maximum of $F_V(D)$ for samples 1 is located at larger D than for samples 2, and the contribution to V'_p from the range of extrapolation is relatively small for samples 1. For mixed samples 1, this contribution ranged from 3% for SAH₁ to 14% for ICE₁, with the exception of 20% for SAN₁. Thus, for these samples the possible error in the estimated contribution of small particles is not expected to introduce large error in the estimate of V'_p . We also note that the V'_p values were very small, generally on the order of 10^{-5} , and in exceptional cases as low as 7.7×10^{-6} for SAN₁. Therefore the $a_w(\lambda)$ term in Eq. 3 could be ignored with no significant effect ($<1\%$) on the calculated $a_{\text{pm}}(\lambda)$.

Knowing $a_{\text{pm}}(\lambda)$ from Eq. 3, the imaginary part of refractive index of particles, $n'(\lambda)$, was calculated from

$$n'(\lambda) = \frac{a_{\text{pm}}(\lambda) \times \lambda}{4\pi} \quad (4)$$

Note that the values of the imaginary refractive index of particles relative to water are lower by $\sim 25\%$ than those calculated with Eq. 4. A simple way to calculate the imaginary index relative to water (which is sometimes reported in oceanographic literature) would be to divide the values from Eq. 4 by 1.34. The value of 1.34 is a reasonable assumption for the real part of the refractive index of water for the wavelength range considered. The imaginary part of the refractive index of water would be neglected in such calculations because of negligibly small values at these wavelengths.

The estimates of $n'(\lambda)$ from Eq. 4 should be interpreted with caution. Because $a_p(\lambda)$, and hence the estimates of $a_{\text{pm}}(\lambda)$, are affected by the package effect, the $n'(\lambda)$ estimates are also affected, so they depend on the size distribution of particles. The essence of this effect in the context of n' determinations is that two assemblages of particles with the same n' and the same V'_p but different particle sizes will produce different absorption coefficients a_p (i.e., lower for larger particles than for smaller ones) and, hence, the different estimates of n' from our calculations. Our determinations of $n'(\lambda)$ were made for mixed samples 1 with a bigger role of the relatively large particles, which ensured a more reliable estimation of V'_p than for samples 2, as discussed above. Thus the $n'(\lambda)$ estimates for samples 1 should be interpreted with due caution as the approximate lower limit for the examined particulate assemblages. Because of the approximate nature of the derivation of n' and weak or negligibly small absorption by samples of single-mineral species, we do not report n' for these samples.

Results and discussion

SPM and POC concentrations—The determinations of SPM and POC indicated that for most samples, organic

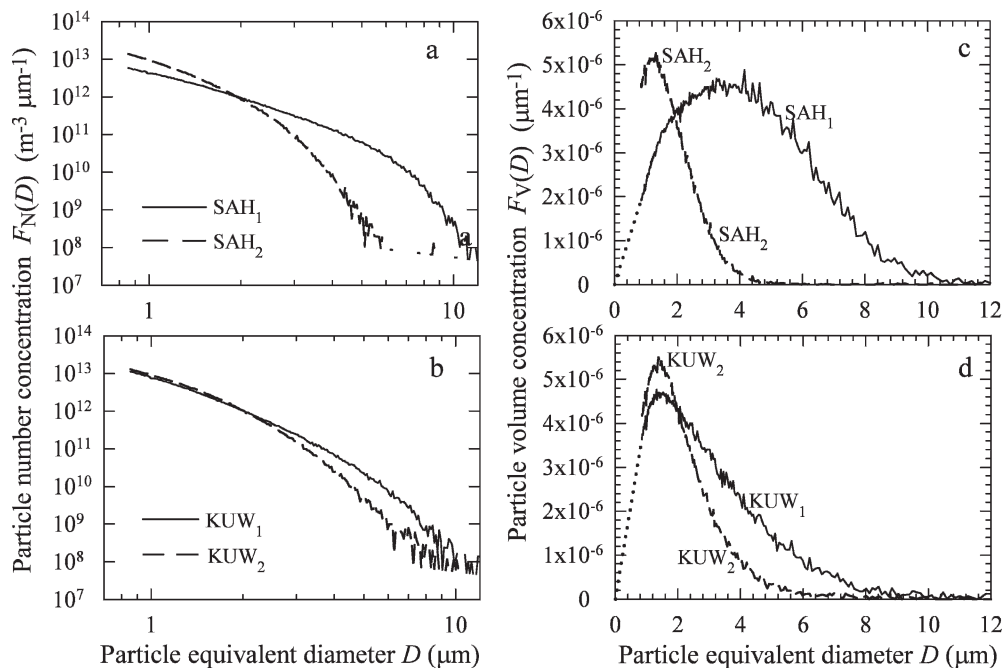


Fig. 1. Density functions of PSD for the samples of Saharan dust (SAH) and soil dust from Kuwait (KUW). (a, b) The functions for particle number concentration, $F_N(D)$; (c, d) the particle volume concentration, $F_V(D)$. The dotted lines show the extrapolation of $F_V(D)$ in the submicrometer size range $D < 0.85 \mu\text{m}$ (i.e., below the level of detection with our instrumentation) for the samples with subscript “1”, for which the imaginary refractive index was estimated (see text for details).

carbon constituted a small fraction ($<3.5\%$) of the total mass of dry particulate matter (Table 1). Because POC can serve as a proxy of particulate organic matter (POM), the data in Table 1 confirm that the samples containing primarily one mineral species (e.g., ILL and MON) as well as the mixed samples SAH, AUS, ICE, and OAH were dominated by mineral particles. Although the organic make-up of the samples is likely variable, one can use an approximate relationship $\text{POM} = 2.6 \times \text{POC}$ (Copin-Montégut 1980) to estimate that the contribution of POM to SPM for these mineral-dominated samples is roughly between 5% (ICE) and 9% (OAH). These estimates represent an approximate upper limit because organic carbon can generally make up 40–50% of POM. The samples NIG, SAN, and KUW cover a broad range of organic–inorganic mixtures. The estimates of the contribution of POM to SPM are 19%, 42%, and 71%, respectively. Thus, for these samples, the organic matter is important or even a dominant component. We also note that the POC:SPM ratio is nearly the same for OAH₁ and OAH₂, although these two samples differed significantly in terms of size distribution and bulk concentrations of SPM and POC. This result suggests that the time periods of particle settling in our experiments had likely a much stronger effect on PSD than composition.

PSD—Figure 1 illustrates differences in the PSD that were produced by sedimentation of particle suspension over different periods of time. We show example results for

the mineral-dominated SAH sample and for the organic-dominated KUW sample. In both cases, significant differences in PSD are observed. For the Saharan dust sample, the differences are particularly large. For example, the maximum of the distribution of particle volume concentration, $F_V(D)$, is shifted from $\sim 4 \mu\text{m}$ (SAH₁) to $1.5 \mu\text{m}$ (SAH₂). For SAH₁, 50% of the total particle volume over the examined size range is contained within the diameter range 0.85–4.07 μm (see D_{V50} in Table 2). For SAH₂, this range is 0.85–1.73 μm . A similar trend in the change of PSD was also observed for other samples, although the changes were not as large as those between SAH₁ and SAH₂. For example, for the Kuwait sample, 50% of the particle volume is contained in the diameter range 0.85–2.75 μm for KUW₁ and 0.85–1.98 μm for KUW₂. Figure 1 also shows that PSD can differ significantly among the various samples that were prepared under similar sedimentation conditions, for example SAH₁ is quite different from KUW₁. These differences are likely attributable to significant variation in PSD and possibly also in particulate composition between the original powder samples. Figure 1c,d also illustrates the extrapolation of $F_V(D)$ in the range $D < 0.85 \mu\text{m}$ for the purposes of calculating V'_p .

If we pool together all PSD data, we observe a broad range in the shape of distributions (Fig. 2). The slope of the distribution of particle number concentration $F_N(D)$ is highly variable between the samples (Fig. 2a). For most samples, this slope also changes significantly with particle

Table 2. Parameters for two different particle size distributions (PSDs), indicated with subscripts “1” and “2” in the sample identifier (ID). D_{N50} , D_{G50} , and D_{V50} are the median particle diameters calculated from the measured PSDs representing the particle number concentration, the particle projected-area concentration, and the particle volume concentration, respectively. D_{V95} is the 95th percentile diameter calculated from PSD representing the particle volume concentration.

ID	D_{N50} (μm)	D_{G50} (μm)	D_{V50} (μm)	D_{V95} (μm)
ILL ₁	1.18	2.19	3.55	8.33
ILL ₂	1.08	1.43	1.95	5.52
KAO ₁	1.28	1.70	2.26	6.87
KAO ₂	1.18	1.62	2.05	5.42
MON ₁	1.57	2.95	4.07	8.09
MON ₂	1.22	1.82	2.50	5.99
CAL ₁	1.21	1.92	2.77	6.87
CAL ₂	1.21	1.66	2.02	3.82
QUA ₁	1.37	2.37	3.25	7.67
SAH ₁	1.35	2.78	4.07	7.98
SAH ₂	1.13	1.44	1.73	3.45
AUS ₁	1.15	1.79	2.78	7.73
AUS ₂	1.16	1.63	2.19	6.64
ICE ₁	1.14	1.75	2.56	6.28
ICE ₂	1.06	1.32	1.62	4.05
OAH ₁	1.18	2.16	3.35	7.60
OAH ₂	0.99	1.18	1.61	9.92
KUW ₁	1.19	1.86	2.75	7.09
KUW ₂	1.17	1.57	1.98	4.83
NIG ₁	1.25	2.81	4.65	10.38
SAN ₁	1.11	1.43	1.87	6.68

diameter D within the examined size range; it is generally much steeper at large D than at small D . For comparison, Fig. 2a shows the slope of the power functions varying as $\sim D^{-3.2}$ and $\sim D^{-4.8}$, which covers a range reported for marine particles (e.g., Bader 1970). The slopes of the various portions of the curves in our experiment range from steeper than -4.8 to less steep than -3.2 . Interestingly, the variations in slope with D for our samples are qualitatively consistent with measurements made on minerogenic particles from a freshwater reservoir with an individual particle analysis technique (Peng and Effler 2007).

Large variations are also observed if the PSDs are expressed in terms of the distribution of particle volume concentration, $F_V(D)$ (Fig. 2b). These distributions typically show a maximum located within the range of diameters from <2 to ~ 4 μm . The $F_V(D)$ distributions also show that the concentrations of relatively large particles (>10 μm in size) is negligibly small. Table 2 provides data for the 95th percentile diameter, D_{V95} , calculated from the $F_V(D)$ curves, which indicate that 95% of total particle volume was associated with particles smaller than ~ 4 – 10 μm . The actual assemblages of soil-derived particles that enter coastal marine environments from river runoff or coastal erosion probably often contain more large particles than our samples. In such environments, the presence of large particles can also be supported by some degree of flocculation. Therefore, under such conditions, the results from our experiments are not meant

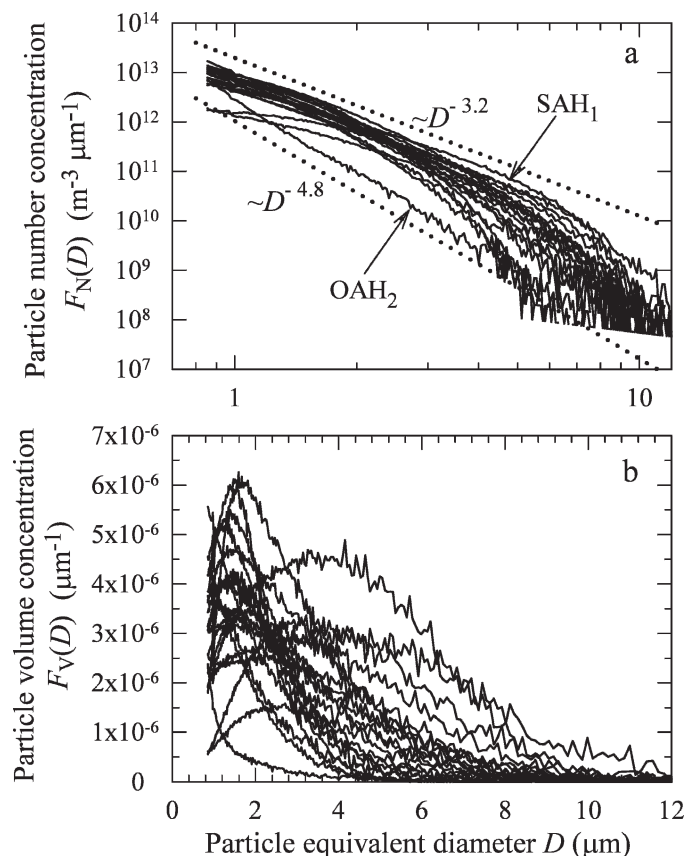


Fig. 2. (a) Density functions of particle number concentration and (b) particle volume concentration for all samples examined (solid lines). The dotted lines in panel a show the power functions with slopes of -3.2 and -4.8 . Also indicated are two example samples: one with a relatively gentle slope (SAH₁) and the other with a steep slope (OAH₂).

to represent the entire assemblages but only their small-sized particulate fraction. We also note that the soil-derived particulate assemblages that enter the ocean via atmospheric deposition or found in offshore environments after transport with currents from coastal areas are expected to be considerably impoverished in large particles. Hence, for such situations, our samples could be more representative of entire assemblages.

Table 2 lists the values of the median particle diameters, which can serve as simple proxies for the shape of the measured PSD. Specifically, D_{N50} , D_{G50} , and D_{V50} indicate the median particle diameters below which we observed 50% of particles in terms of particle number concentration, the particle projected-area concentration, and the particle volume concentration, respectively. We recall that the lower limit of D in these calculations is 0.85 μm . The SAH₂, ICE₂, and OAH₂ samples are characterized by a higher percentage of small-sized particles compared with most other samples. The median diameters for these samples are generally smaller than for other samples. In contrast, the median diameters for NIG₁, SAH₁, ILL₁, and MON₁ are highest among the examined samples, which indicates that the role of small-sized particles was the lowest in these samples.

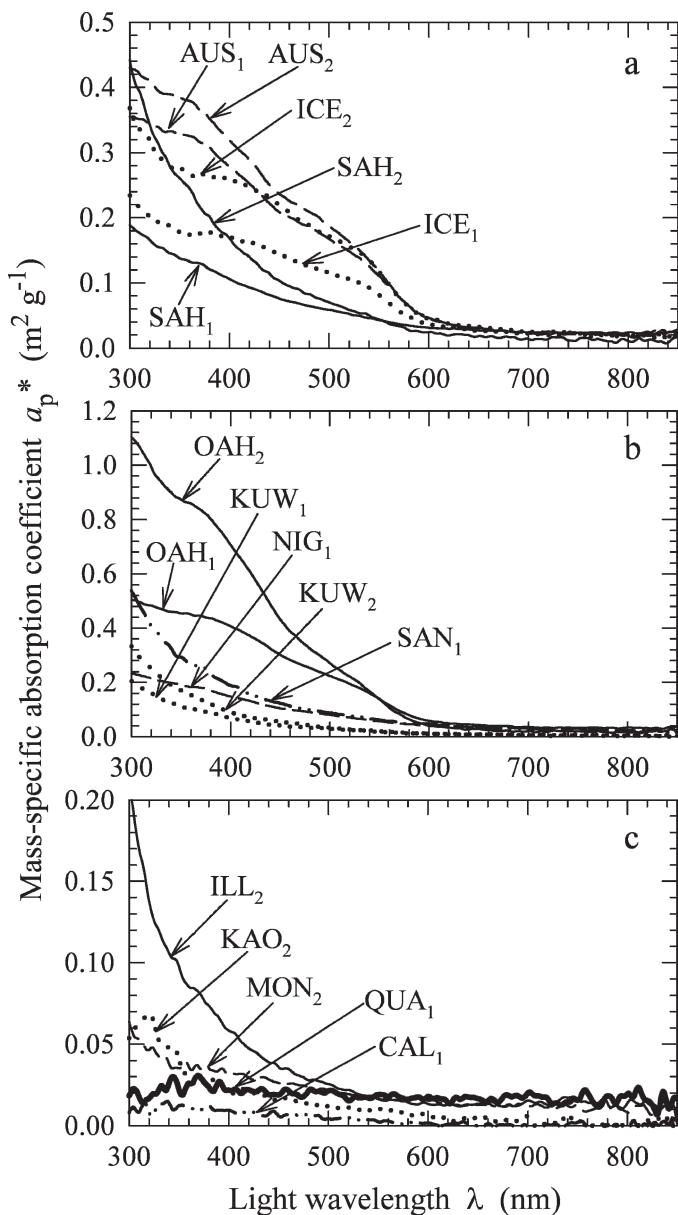


Fig. 3. (a, b) Spectra of mass-specific absorption coefficient of particles for samples of mixed particulate assemblages and (c) for samples of single-mineral species.

Absorption and imaginary refractive index—The broad range of PSDs shown in Fig. 2 is naturally expected to have a major effect on the measured optical properties. Figure 3 illustrates the variability in the mass-specific absorption coefficient, $a_p^*(\lambda)$. For analyzing the effects of PSD, it is best to compare the pairs of samples derived from the same original powder sample, for example, SAH₁ and SAH₂. In this kind of comparison, the source of optical variability associated with variation in particulate composition and refractive index is minimized. There exists a consistent pattern for all pairs of samples being compared in Fig. 3. Samples 1 show lower values of $a_p^*(\lambda)$ compared with samples 2. This is consistent with the package effect as $a_p^*(\lambda)$ decreases with an increase in particle size. The

significance of this result stems from our measurements having been made on mineral-dominated assemblages that generally consist of real nonspherical and internally heterogeneous particles, whereas present theoretical understanding of the package effect is essentially based on models for homogeneous spheres developed in the context of phytoplankton cells (e.g., Morel and Bricaud 1981). In that regard, it is important to note that the internal structure of mineral particles can be quite complex in terms of the localization and distribution of iron, the major pigmenting agent of the particles, because iron can occur as a surface coating or an element of mineral lattice, or it can form crystals of oxides. In our data, the package effect associated with PSD is particularly well seen in the UV and blue spectral regions, where the examined particles exhibit significant absorption. For example, a_p^* at 400 nm for SAH₂ is about 61% higher than for SAH₁ (Fig. 3a). This change is associated with ~57% reduction in the size parameter D_{V50} for SAH₂ compared with SAH₁ (Table 2). Generally, smaller changes in PSD correspond to smaller changes in $a_p^*(\lambda)$. For example, for the Australian sample, these changes were relatively small; that is, a 21% decrease in D_{V50} was accompanied by a 16% increase in $a_p^*(400)$ between AUS₁ and AUS₂.

The sample from Oahu shows the highest overall magnitude of $a_p^*(\lambda)$ (Fig. 3b), which is apparently associated with high iron content in these particles. There is also a large difference in $a_p^*(\lambda)$ between OAH₁ and OAH₂. The value of $a_p^*(400)$ for OAH₂ is higher by 77% than for OAH₁. If we exclude from consideration the data for single-mineral species (Fig. 3c), the samples from Kuwait (KUW₁ and KUW₂) show the lowest $a_p^*(\lambda)$ (Fig. 3b). These samples had the highest organic content among the samples examined. A comparison of results presented in Fig. 3 with field data from mineral-dominated coastal waters indicates that $a_p^*(\lambda)$ for most of our samples of mixed assemblages is higher than the values obtained from field experiments (Bowers et al. 1996; Babin et al. 2003b; McKee and Cunningham 2006). These differences likely result, at least partly, from a smaller contribution of relatively large particles in our samples compared with field samples.

For most samples presented in Fig. 3a,b, the shape of the absorption spectrum shows some features, such as shoulders and changes in slope, that are superimposed on a general decrease of absorption with wavelength. These features suggest that the actual measured curves can locally depart substantially from an exponential function, which has often been used to describe the absorption spectra of nonphytoplankton particles referred to commonly as detritus (e.g., Roesler et al. 1989; Bricaud and Stramski 1990). Despite the presence of irregularities in the spectral shapes, we have examined the exponential fits for our mixed samples. The steepest slopes of -0.00953 and -0.00881 (on the basis of the entire spectral range 300–850 nm) were found for OAH₂ and KUW₂ samples, respectively. The SAH₁ and NIG₁ samples had the least steep slopes of -0.00412 and -0.00463 , respectively. This range of slopes tends to be at the lower end of the values reported in the literature for absorption by detritus. For example, Roesler et al. (1989, *see* their table 1) assumed the

slope of -0.011 as a satisfactory “mean” value for the detrital absorption spectrum, although they also indicated a range of variability from -0.006 to -0.014 .

The samples of single-mineral species show very weak absorption—in some cases, below the level of meaningful detection with our measurement system (Fig. 3c). The illite sample with the highest absorption in Fig. 3c, ILL_2 , was still less absorbing than KUW_1 , which showed the lowest absorption among the mixed particulate assemblages. Whereas the estimate of $a_p^*(400)$ for KUW_1 is $0.0683 \text{ m}^2 \text{ g}^{-1}$, it is $0.0583 \text{ m}^2 \text{ g}^{-1}$ for ILL_2 . The estimate of absorption spectrum for the quartz sample QUA_1 in Fig. 3c is an overestimate of actual absorption by pure quartz. Like calcite, pure quartz exhibits extremely weak absorption within the examined spectral range, which is expected to be below the level of detection with our instrumentation. The estimates of $a_p^*(\lambda)$ for QUA_1 in Fig. 3c are, however, between 0.015 and $0.02 \text{ m}^2 \text{ g}^{-1}$. These relatively high values are most likely caused by inadequate correction of measurements of QUA_1 with Eq. 1, in which we assumed $\alpha = -0.05$ from determinations with calcite samples. A value of -0.03 for α would satisfy the likely scenario that the QUA_1 sample had no detectable absorption.

The differences in α for practically nonabsorbing calcite and quartz samples suggest that no unique baseline representing true zero absorption—that is, in effect, no unique spectrum of $\alpha(\lambda)$ —can be established from measurements of different particulate samples with our measurement system. This limitation is, in fact, common for various instrumentations for measuring absorption of scattering samples. Such an ideal baseline is not realistically obtainable because it would have to perfectly eliminate errors associated with differences in the amount of undetected photons from the scattering and reflection processes between reference and sample measurements for different types of samples (i.e., different PSDs and particulate compositions). This problem makes it difficult to accurately quantify absorption whenever absorption is weak, which is one of the main reasons for a debate on the question of near-IR absorption by marine particles (e.g., Babin and Stramski 2002; Tassan and Ferrari 2003; Bowers and Binding 2006). In actuality, there appears to be no simple answer to this question because seawater might contain a great diversity of particle types with different optical properties. These types range from particles that have negligible absorption in the near-IR, like much organic matter, to particles that can absorb very efficiently, like black elemental carbon originating from natural combustion processes (forest and grassland fires) and anthropogenic contributions (fossil fuel combustion) (Lindberg et al. 1993). In view of such diversity, indiscriminate generalizations with regard to near-IR absorption do not seem to be warranted. The origins of near-IR absorption by assemblages of marine particles require better understanding. Some mineral particles have been suggested as a source of near-IR absorption in field samples (e.g., Tassan and Ferrari 2003; Bowers and Binding 2006) but further analysis of this question, including the assessment of the role of other constituents, especially black carbon, is

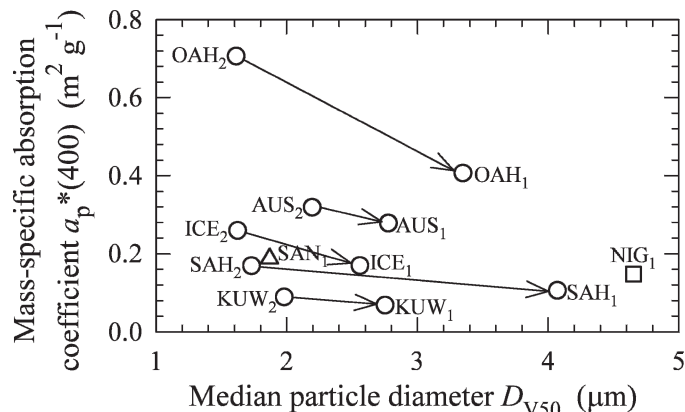


Fig. 4. The mass-specific absorption coefficient of particles at 400 nm as a function of median particle diameter calculated from the size distributions of particle volume concentration. The data for samples of the mixed particulate assemblages are shown. The arrows show a decrease in $a_p^*(400)$ associated with a change in PSD.

needed. Although the role of black carbon in marine optics has not been studied, these particles were found in significant amounts in marine sediments (Middelburg et al. 1999), and their presence can be expected in seawater (Kaneyasu and Murayama 2000; Mitra et al. 2002).

For our samples of the mixed particulate assemblages presented in Fig. 3a,b, the estimates of a_p^* in the near-IR are usually close to $0.02 \text{ m}^2 \text{ g}^{-1}$. If we disregard the organic-dominated KUH samples, $a_p^*(800)$ has an average value of $0.0207 \text{ m}^2 \text{ g}^{-1}$ and a range from $0.0107 \text{ m}^2 \text{ g}^{-1}$ for SAH_2 to $0.034 \text{ m}^2 \text{ g}^{-1}$ for OAH_1 . The KUH samples have much lower values of $a_p^*(800)$ within the range $3\text{--}5 \times 10^{-3} \text{ m}^2 \text{ g}^{-1}$. The ratio of blue (400 nm) to near-IR (800 nm) absorption for the mixed samples ranges from ~ 4.4 (SAH_1) to ~ 40 (OAH_2), with an average value of ~ 15 . Thus, for most samples, absorption at 800 nm was $<10\%$ of the absorption at 400 nm. These results are quite consistent with our earlier determinations of near-IR absorption (Babin and Stramski 2004; Stramski et al. 2004b).

One can expect a priori that the variability in a_p^* shown in Fig. 3 cannot be explained by variations in PSD alone. This is supported by comparison of changes in a_p^* as a function of D_{V50} for the mixed samples (Fig. 4). We have chosen to show a_p^* at 400 nm, where absorption is significant for all mixed samples. Whereas the particle size effect is reflected in a decrease of $a_p^*(400)$ with D_{V50} for each pair of samples, variability is also large in $a_p^*(400)$ among the samples at the same values of D_{V50} . For example, for D_{V50} close to $2 \mu\text{m}$, $a_p^*(400)$ for the OAH particles is ~ 10 times higher than for the KUH particles. To first approximation, we can assume that the samples with the same D_{V50} have PSDs with a similar shape. Thus, large differences in a_p^* at the same D_{V50} suggest that different samples have different capacity to absorb light because of differences in particle composition; hence, the samples have different values of the imaginary refractive index $n''(\lambda)$.

This suggestion is supported in Fig. 5, which provides a comparison of our estimates of $n''(\lambda)$ for AUS_1 , ICE_1 , SAH_1 , OAH_1 , KUH_1 , NIG_1 , and SAN_1 . As could have

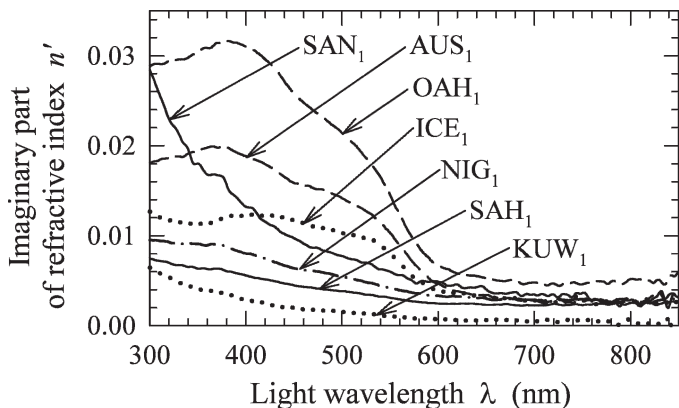


Fig. 5. Spectra of imaginary part of refractive index of particles for samples of mixed particulate assemblages. The data represent estimates of the approximate lower limit of the imaginary refractive index, which were obtained for samples with subscript "1" (see text for details).

been expected from Figs. 3, 4, the sample OAH₁ shows the highest and KUW₁ the lowest $n'(\lambda)$. At 400 nm, n' ranges from 0.0029 for KUW₁ to 0.031 for OAH₁. Although we are not aware of similar $n'(\lambda)$ data for mineral-rich particulate assemblages from aquatic environments, it is instructive to make comparisons with existing data on nonliving aquatic particles. A few determinations for marine detrital particles from the Sargasso Sea showed that those particles were relatively weak absorbers of light (Stramski and Woźniak 2005). The n' values for those particles were usually on the order of 10^{-4} and as high as 0.0033 at 400 nm for one of the samples (note that the original results reported in that article represented the imaginary index relative to water rather than the absolute index in vacuum, which is reported in this study). The n' values for detrital particles from the Sargasso Sea are below or near the lower end of the range from this study. We note that these detrital particles were almost certainly organic and originated from marine biological activities. In general, however, n' of nonliving organic particles is not necessarily constrained to such low values (Woźniak et al. 2005).

Compared with nonliving aquatic particles, more information is available in the literature about $a_{\text{pm}}(\lambda)$, or equivalently $n'(\lambda)$, of atmospheric particulate matter. One can expect a significant overlap in the composition of atmospheric particulate matter and the category of aquatic particulate matter of interest to our study because both particulate pools are composed largely of soil-derived materials. Our results in Fig. 5 fall within a broad range of $n'(\lambda)$ reported in the literature for atmospheric particulate matter (Gillespie and Lindberg 1992; Sokolik et al. 1993; Dubovik et al. 2002). The higher values of n' on the order of 10^{-2} were typically reported for urban/industrial and biomass burning aerosols. The lower values generally on the order of 10^{-3} , but extending to >0.01 , were reported in less populated rural areas and for the aerosol type referred to as desert dust. Our estimates of n' for the SAH₁ sample (e.g., 0.0074 at 300 nm, 0.0056 at 400 nm, and 0.0022 at 700 nm) are between the relatively high estimates for Saharan dust obtained by Patterson et al. (1977) and

the relatively low estimates for desert dust derived by Dubovik et al. (2002). The broad range of n' can be explained in terms of some important categories of materials that make up the atmospheric particulate matter. The bulk of this matter could be considered to be composed of weak absorbers in the visible and near-IR, such as quartz, calcite, silicate clay minerals, and several simple salts. Added to this mixture is the small (but highly variable) amounts of strong absorbers, such as oxides of iron and black carbon (Lindberg 1975; Lindberg et al. 1993; Sokolik and Toon 1999).

Several samples of mixed particulate assemblages examined in this study show a clear transition from strong absorption in the ultraviolet and blue to weak absorption in the red and near-IR (Fig. 5). This feature is most remarkable in the n' spectra for mineral-dominated samples from Oahu and Australia, and it suggests a major role of iron oxides. Our earlier study showed, for example, that iron contributed about 5, 6, and 17% to the total dry mass of particles for the Saharan, Spitsbergen, and Australian dust samples, respectively (Babin and Stramski 2004). Oxides of iron, such as ferrous oxide (Fe_2O_3), which is a common impurity in most natural mineral matter, are known to exhibit a transition from a strong to a weak absorber at the ~ 500 – 600 nm wavelength range (Lindberg et al. 1993; Sokolik and Toon 1999). Compared with mineral-dominated samples that are apparently rich in iron oxides (SAH₁, AUS₁, ICE₁, and OAH₁), the samples with high organic content, especially KUW₁, are characterized by a more gradual decrease of n' with wavelength.

Summarizing the sources of absorption in our samples, it appears that the significantly higher absorption of mixed particulate assemblages compared with the samples of single-mineral species (see Fig. 3), especially in the ultraviolet and blue regions, can be attributed primarily to iron content of the mixed samples and, for some samples, to significant organic matter content. Some, albeit minor, role of other strongly absorbing compounds in the mixed samples, especially black carbon, is difficult to assess but cannot be excluded. For example, the atmospheric dust sample SAN₁ is probably a fairly complex mixture of particle types that include desert dust containing iron oxides mixed not only with organic matter but possibly also with some contribution from urban aerosol containing black carbon.

Scattering and single-scattering albedo—Differences in the size distribution and composition of particles are also responsible for considerable variations in light-scattering properties of particulate assemblages. The patterns of variability in magnitude and spectral shape of the mass-specific scattering coefficient $b_p^*(\lambda)$ are quite intricate (Fig. 6). The $b_p^*(\lambda)$ values generally range between 0.5 and $1.5 \text{ m}^2 \text{ g}^{-1}$. In a few cases, the $b_p^*(\lambda)$ values were outside this range. For example, the calcite sample, CAL₂, showed the strongest scattering among the samples, with $b_p^*(\lambda)$ exceeding $1.5 \text{ m}^2 \text{ g}^{-1}$ in the blue and ultraviolet. The relatively high refractive index of calcite compared with other mineral species (e.g., Kerr 1977) could be partly responsible for this result. On the basis of all mixed samples

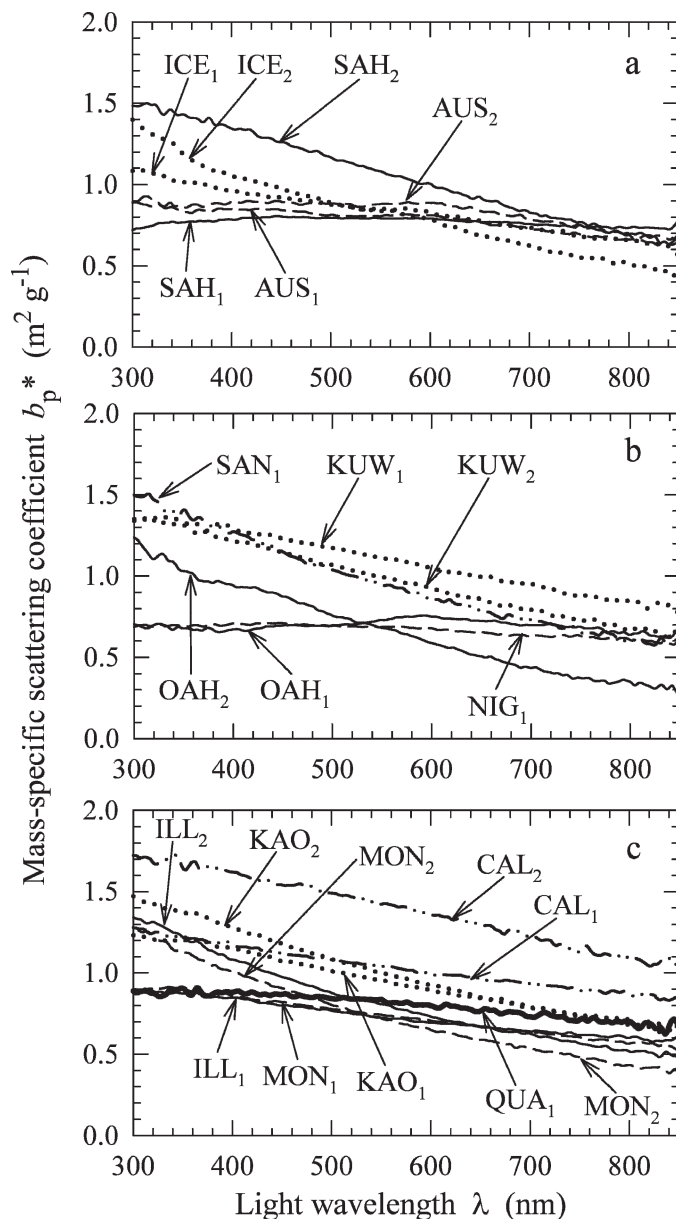


Fig. 6. (a, b) Spectra of the mass-specific scattering coefficient of particles for samples of mixed particulate assemblages and (c) for samples of single-mineral species.

(Fig. 6a,b), the average b_p^* at 400, 550, and 800 nm is 1.0, 0.87, and $0.64 \text{ m}^2 \text{ g}^{-1}$, respectively. If the data for the samples of single-mineral species are included in the calculations, these average values increase by just a few percent. The variability in $b_p^*(\lambda)$ between the samples is significant in that the coefficient of variation on the basis of all data from Fig. 6 exceeds 20% at each wavelength. Interestingly, most scattering spectra for the mixed samples (Fig. 6a,b) converge in the near-IR spectral region. Upon ignoring three samples—ICE₂, OAH₂, and KUW₁—the average b_p^* at 800 nm is $\sim 0.67 \text{ m}^2 \text{ g}^{-1}$ (as opposed to $0.64 \text{ m}^2 \text{ g}^{-1}$ for all mixed samples), but the coefficient of variation is now reduced to only 6.4%.

The magnitude of $b_p^*(\lambda)$ in Fig. 6 is relatively high compared with most estimates from the literature for marine particulate assemblages rich in minerals. For several coastal and shelf marine environments, the determinations of b_p^* produced values close to or $< 0.5 \text{ m}^2 \text{ g}^{-1}$ in the green part of the spectrum (Babin et al. 2003a; Bowers and Binding 2006; McKee and Cunningham 2006). Theoretical modeling shows that the increased proportion of large particles, increased proportion of high-density mineral particles, or both will reduce the magnitude of b_p^* (Babin et al. 2003a; Woźniak and Stramski 2004). The relatively high values of b_p^* in our experiments appear to result primarily from steep slopes of size distribution for $D > 3\text{--}5 \mu\text{m}$, and hence, a very small contribution of larger particles (see Fig. 2; Table 2).

The dominance of small-sized particles is also responsible for the spectral trend of $b_p^*(\lambda)$ to decrease with λ for most samples (Fig. 6). Several samples showed, however, weak spectral dependence or nearly flat spectral curves of scattering (e.g., SAH₁, OAH₁, and NIG₁). The spectral slope η obtained by a power function fit of the form $b_p^*(\lambda) \propto \lambda^{-\eta}$ is presented versus the particle size parameter D_{G50} in Fig. 7. As expected, there is a pattern of a decrease in η with increasing D_{G50} . The data for the mixed samples and single-mineral species follow a similar pattern, although the montmorillonite samples (MON₁ and MON₂) are the evident exception. The MON samples show steeper slopes than the general trend of η versus D_{G50} would suggest. This is most likely associated with the relatively more submicrometer particles, below the level of detection of our particle sizing instrument ($< 0.85 \mu\text{m}$), contained in the montmorillonite samples. These very small particles contribute to scattering but are excluded from the calculations of D_{G50} . Note also that if samples 1 are compared with their sample 2 counterparts, the steeper slopes η are generally observed for those of samples 2, as expected from the differences in size distributions.

Further generalizations about the variability in $b_p^*(\lambda)$ are difficult because the patterns shown in Fig. 6 are complex. For example, the values of b_p^* for SAH₂ are higher than those for SAH₁ for most of the spectral region, so that the curves for SAH₁ and SAH₂ cross each other in the near-IR spectral region. The opposite pattern is observed for the Kuwait samples, with the spectra crossing each other in the ultraviolet. The intermediate case is observed for the spectra of Oahu samples, which cross each other in the green part of the spectrum. These intricate patterns reflect the dependence of scattering on the PSD and other particle properties, especially the real and imaginary parts of the refractive index.

A simple dimensionless optical parameter that combines the absorption and scattering properties is the single-scattering albedo, which is the ratio of the scattering coefficient to the sum of scattering and absorption coefficients. This parameter is particularly useful for optical/radiative transfer modeling. The spectra of single-scattering albedo of particles, $\omega_{\text{op}}(\lambda)$, for the mixed samples are shown in Fig. 8. Because of low absorption in the near-IR, the values of $\omega_{\text{op}}(\lambda)$ in this spectral region are high (> 0.95), indicating that the probability of near-IR photon

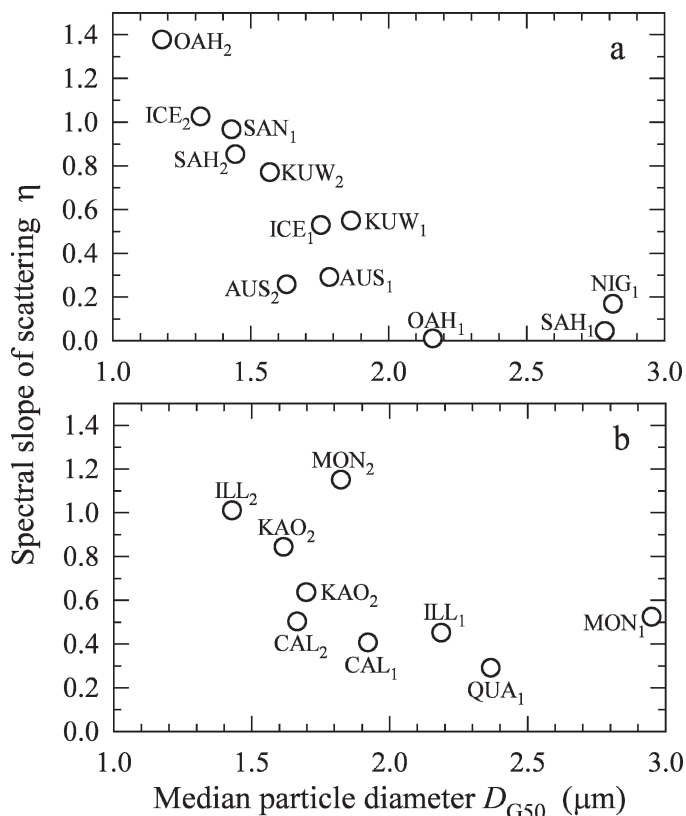


Fig. 7. (a) Spectral slope of the particulate scattering coefficient as a function of median particle diameter calculated from the size distributions of particle projected-area concentration for samples of mixed particulate assemblages and (b) for samples of single-mineral species.

survival on the interaction with particles is $>95\%$. Significant differences between the samples are observed at shorter wavelengths. For example, for relatively weakly absorbing samples from Kuwait, $\omega_{\text{op}}(\lambda)$ in the blue is relatively high, >0.9 , and drops below that value only in the ultraviolet range. In contrast, for strongly absorbing samples from Oahu, $\omega_{\text{op}}(\lambda)$ is as low as ~ 0.6 at blue wavelengths and drops below that value at ultraviolet wavelengths.

POC-specific optical coefficients—To illustrate the limitation of optical proxies of POC for particulate assemblages that vary largely in composition from mineral-dominated to organic-dominated, we briefly report on the POC-specific absorption and scattering coefficients. As expected, the POC-specific coefficients were lowest for organic-dominated samples. For example at 400 nm, the POC-specific absorption was as low as $0.329 \text{ m}^2 (\text{g C})^{-1}$ for the most organic sample from Kuwait. For mineral-dominated samples from Spitsbergen, Australia, and Oahu, these values were much greater, in the range of ~ 10 to $20 \text{ m}^2 (\text{g C})^{-1}$. Similarly, POC-specific scattering varied greatly, from $\sim 3.65 \text{ m}^2 (\text{g C})^{-1}$ at 550 nm for the Kuwait sample to $20\text{--}50 \text{ m}^2 (\text{g C})^{-1}$ for the mineral-dominated samples. These results support the view that POC cannot be estimated directly from POC-specific

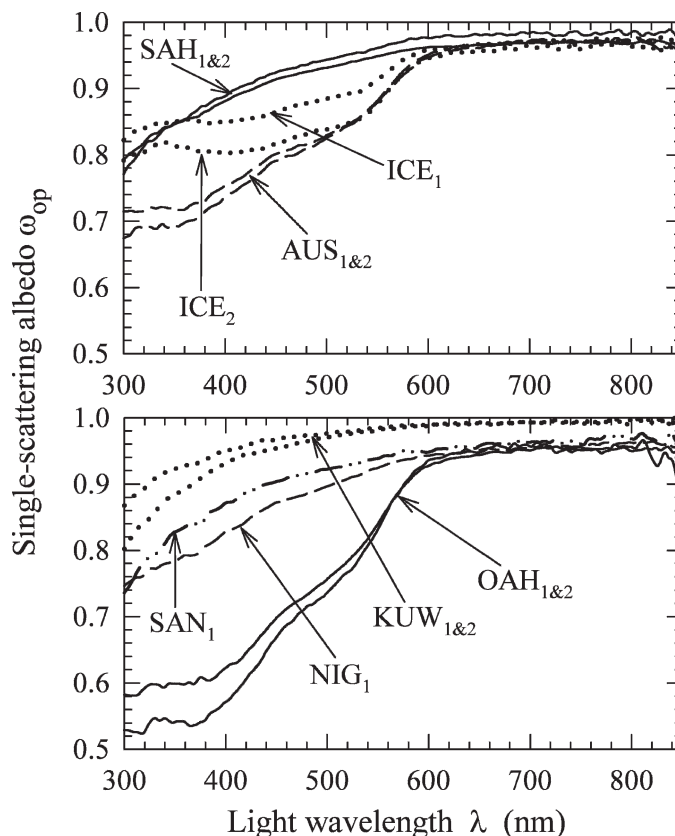


Fig. 8. Spectra of the single scattering albedo of particles for samples of mixed particulate assemblages.

optical coefficients in waters with significant and variable amounts of minerogenic particles.

Our study provides quantitative evidence that the mass-specific absorption and scattering coefficients for particulate matter originating from land can vary substantially because of variability in PSD and the origin of soil. Understanding of the roles of various particle types in hydrologic optics is still very limited because the common traditional approach has been to measure the bulk optical properties along with a few bulk properties of particulate populations, such as the bulk Chl *a* concentration or bulk mass concentration of particulate matter, which cannot adequately explain the optical variability observed in natural waterbodies.

We believe that building the base of knowledge about various optically and biogeochemically important particle types within an alternative framework, referred to as the reductionist approach (*see* Stramski et al. 2001; 2004a), is a prerequisite for advancing the mechanistic understanding of natural optical variability and for developing improved applications of optics, including remote sensing of aquatic environments. As an example, one can envision the development of an improved inverse reflectance model that would solve simultaneously for a number of component IOPs and associated water constituents, including a number of optically and biogeochemically important particle types. Such a model could be based on extensive forward radiative transfer simulations to

generate a library of reflectance spectra corresponding to a very large number of various combinations of water column IOPs, represented as a sum of contributions associated with various particle types defined with a reductionist model. These ideas of forward modeling were demonstrated for a limited number of particle types in preliminary studies by Mobley and Stramski (1997) and Stramski and Mobley (1997). For inverse applications, the precomputed library could then be used as a look-up table for matching the magnitude and spectral shape of precomputed high-resolution reflectance spectra with the measured reflectance (Mobley et al. 2005) to provide a simultaneous solution for a number of component IOPs and associated particle type concentrations. It is conceivable that this approach, with additional support of observational constraints, would be effective for circumventing the ambiguity problem of the present inverse ocean color models that involve just a few bulk IOPs and a few bulk particle types (Defoin-Platel and Chami 2007).

At present, we must accept that this approach will require a significant period of time before the partitioning of particulate assemblages into a certain manageable number of optically and biogeochemically important particle functional types can be fully applied to actual marine and freshwater environments in the optical/biogeochemical modeling or remote sensing context. Such advancements need an increased mechanistic understanding of which particle types and to what extent the different particle types influence optics in various environments, how optics relates to the physicochemical characteristics of real particles, how optics responds to particle dynamics, and how such mechanisms can be included in regional and global models. We believe that basic laboratory studies of particle types and field studies in which optical measurements are taken in tandem with a detailed characterization of particle populations with the use of various techniques, including, especially, individual particle analysis, must be pressed further and must be better coordinated. The number and specification of particle types that are required for a fully functional reductionist approach in any particular aquatic environment or in the global ocean are not known at present. Therefore, at this early stage, it is justifiable to include in the laboratory experiments the various types of particles of different origins, especially those for which quantitative information about optical properties and their relation to particle physicochemical characteristics is lacking. This work is our contribution to such laboratory studies. Significant enhancements of such studies are still required; for example, the characterization of particle physicochemical properties could be significantly improved compared with our study, and the addition of measurements of angular scattering patterns would be desirable. With regard to field studies, an example that embraces the reductionist approach is the recent work by Peng and Effler (2007). By applying scanning electron microscopy interfaced with X-ray microanalysis and image analysis, these investigators measured the composition, size, shape, and concentration of organic and several minerogenic particle types present in a freshwater reservoir. These measurements were used

as input to a Mie scattering model, which provided an estimate of light scattering budget associated with these particle types. In another field study, flow cytometry measurements of individual particles were combined with Mie scattering calculations to determine the effects of several particle types on the IOPs of Atlantic shelf waters off New England (Green et al. 2003).

Laboratory studies like the one described in this paper, our earlier work with plankton cultures summarized in Stramski et al. (2001), and field studies like those by Peng and Effler (2007) and Green et al. (2003) can be viewed as example precursor work that lays out the strategy for advancing the reductionist approach in hydrologic optics. When such studies produce sufficient knowledge about the properties, abundances, and dynamics of particle types in various environments, it might be possible to know the level of complexity of particulate assemblages at a level manageable in the modeling and remote sensing context, which will successfully reproduce the observed optical variability in specific regions of interest.

References

- ALLEN, T. 1981. Particle size measurement, 3rd ed. Chapman and Hall.
- ARIMOTO, R., W. L. BALSAM, AND C. SCHLOESSLIN. 2002. Visible spectroscopy of aerosol particles collected on filters: Iron-oxide minerals. *Atmos. Environ.* **36**: 89–96.
- BABIN, M., A. MOREL, V. FOURNIER-SICRE, F. FELL, AND D. STRAMSKI. 2003a. Light scattering properties of marine particles in coastal and open ocean waters as related to the particle mass concentration. *Limnol. Oceanogr.* **48**: 843–859.
- , AND D. STRAMSKI. 2002. Light absorption by aquatic particles in the near-infrared spectral region. *Limnol. Oceanogr.* **47**: 911–915.
- , AND ———. 2004. Variations in the mass-specific absorption coefficient of mineral particles suspended in water. *Limnol. Oceanogr.* **49**: 756–767.
- , ———, G. M. FERRARI, H. CLAUSTRE, A. BRICAUD, G. OBOLENSKY, AND N. HOEPFFNER. 2003b. Variations in the light absorption coefficients of phytoplankton, non-algal particles, and dissolved organic matter in coastal waters around Europe. *J. Geophys. Res.* **108**: 3211, doi:10.1029/2001JC000882.
- BADER, H. 1970. The hyperbolic distribution of particle size. *J. Geophys. Res.* **75**: 2822–2830.
- BEUSEN, A. W. H., A. L. M. DEKKERS, A. F. BOUWMAN, W. LUDWIG, AND J. HARRISON. 2005. Estimation of global river transport of sediments and associated particulate C, N, and P. *Glob. Biogeochem. Cycles* **19**: GB4S05, doi:10.1029/2005GB002453.
- BOWERS, D. G., AND C. E. BINDING. 2006. The optical properties of mineral suspended particles: A review and synthesis. *Estuar. Coast. Shelf Sci.* **67**: 219–230.
- , G. E. L. HARKER, AND B. STEPHAN. 1996. Absorption spectra of inorganic particles in the Irish Sea and their relevance to remote sensing of chlorophyll. *Int. J. Remote Sens.* **17**: 2449–2460.
- BRICAUD, A., A.-L. BEDHOMME, AND A. MOREL. 1988. Optical properties of diverse phytoplanktonic species: Experimental results and theoretical predictions. *J. Plankton Res.* **10**: 851–873.

- , AND A. MOREL. 1986. Light attenuation and scattering by phytoplanktonic cells: A theoretical modelling. *Appl. Opt.* **25**: 571–580.
- , AND L. PRIEUR. 1983. Optical efficiency factors of some phytoplankters. *Limnol. Oceanogr.* **28**: 816–832.
- , AND D. STRAMSKI. 1990. Spectral absorption coefficients of living phytoplankton and nonalgal biogenous matter: A comparison between the Peru upwelling area and the Sargasso Sea. *Limnol. Oceanogr.* **35**: 562–582.
- CARDER, K. L., R. G. STEWARD, P. R. BETZER, D. L. JOHNSON, AND J. M. PROSPERO. 1986. Dynamics and composition of particles from an aeolian input event to the Sargasso Sea. *J. Geophys. Res.* **91**: 1055–1066.
- COPIN-MONTEGUT, G. 1980. Matière en suspension dans les eaux de mer: répartition, composition chimique, origine et évolution. Ph.D. thesis, Laboratoire de Physique et Chimie Marines, Université Pierre et Marie Curie.
- DEATON, B. C., AND W. L. BALSAM. 1991. Visible spectroscopy—a rapid method for determining hematite and goethite concentration in geological materials. *J. Sediment Petrol.* **61**: 628–632.
- DEFOIN-PLATEL, M., AND M. CHAMI. 2007. How ambiguous is the inverse problem of ocean color in coastal waters? *J. Geophys. Res.* **112**: C03004, doi:10.1029/2006JC003847.
- DUBOVIK, O., AND OTHERS. 2002. Variability of absorption and optical properties of key aerosol types observed in worldwide locations. *J. Atmos. Sci.* **59**: 590–608.
- DUYSENS, L. N. M. 1956. The flattening of the absorption spectrum of suspensions as compared to that of solutions. *Biochim. Biophys. Acta* **19**: 1–12.
- GILLESPIE, J. B., AND J. D. LINDBERG. 1992. Seasonal and geographical variations in imaginary index of atmospheric particulate matter. *Appl. Opt.* **31**: 2107–2111.
- GREEN, R. E., H. M. SOSIK, R. J. OLSON, AND M. D. DURAND. 2003. Flow cytometric determination of size and complex refractive index for marine particles: Comparison with independent and bulk estimates. *Appl. Opt.* **42**: 526–541.
- HAARDT, H., AND H. MASKE. 1987. Specific in vivo absorption coefficient of chlorophyll *a*. *Limnol. Oceanogr.* **32**: 608–619.
- HALE, G. M., AND M. R. QUERRY. 1973. Optical constants of water in the 200 nm to 200 μ m wavelength region. *Appl. Opt.* **12**: 555–563.
- KANEYASU, N., AND S. MURAYAMA. 2000. High concentrations of black carbon over middle latitudes in the North Pacific Ocean. *J. Geophys. Res.* **105**: 19881–19890.
- KERR, P. F. 1977. *Optical mineralogy*. McGraw-Hill.
- LERMAN, A., K. L. CARDER, AND P. R. BETZER. 1977. Elimination of fine suspensoids in the oceanic water column. *Earth Planet. Sci. Lett.* **37**: 61–70.
- LINDBERG, J. D. 1975. The composition and optical absorption coefficient of atmospheric particulate matter. *Opt. Quantum Electron.* **7**: 131–139.
- , R. E. DOUGLASS, AND D. M. GARVEY. 1993. Carbon and the optical properties of atmospheric dust. *Appl. Opt.* **32**: 6077–6081.
- , ———, AND ———. 1999. Atmospheric particulate absorption and black carbon measurement. *Appl. Opt.* **38**: 2369–2376.
- McKEE, D., AND A. CUNNINGHAM. 2006. Identification and characterisation of two optical water types in the Irish Sea from in situ inherent optical properties and seawater constituents. *Estuar. Coast. Shelf Sci.* **68**: 305–316.
- MIDDELBURG, J. J., J. NIEUWENHUIZE, AND P. VAN BRUEGEL. 1999. Black carbon in marine sediments. *Mar. Chem.* **65**: 245–252.
- MITRA, S., T. S. BIANCHI, B. A. McKEE, AND M. SUTULA. 2002. Black carbon from the Mississippi River: Quantities, sources, and potential implications for the global carbon cycle. *Environ. Sci. Technol.* **36**: 2296–2302.
- MOBLEY, C. D., AND D. STRAMSKI. 1997. Effects of microbial particles on oceanic optics: Methodology for radiative transfer modeling and example simulations. *Limnol. Oceanogr.* **42**: 550–560.
- , L. K. SUNDMAN, C. O. DAVIS, AND OTHERS. 2005. Interpretation of hyperspectral remote-sensing imagery by spectrum matching and look-up tables. *Appl. Opt.* **44**: 3576–3592.
- MOREL, A., AND A. BRICAUD. 1981. Theoretical results concerning light absorption in a discrete medium, and application to specific absorption of phytoplankton. *Deep-Sea Res.* **28**: 1375–1393.
- PATTERSON, E. M., D. A. GILLETTE, AND B. H. STOCKTON. 1977. Complex index of refraction between 300 and 700 nm for Saharan aerosols. *J. Geophys. Res.* **82**: 3153–3160.
- PENG, F., AND S. W. EFFLER. 2007. Suspended minerogenic particles in a reservoir: Light-scattering features from individual particle analysis. *Limnol. Oceanogr.* **52**: 204–216.
- PETERSON, J. T., AND J. A. WEINMAN. 1969. Optical properties of quartz dust particles in infrared wavelengths. *J. Geophys. Res.* **28**: 6947–6952.
- POPE, R. M., AND E. S. FRY. 1997. Absorption spectrum (380–700 nm) of pure water. II. Integrating cavity measurements. *Appl. Opt.* **36**: 8710–8723.
- RAPHAEL, M. N. 2003. The Santa Ana winds of California. *Earth Interact.* **7**: 1–13.
- ROESLER, C. S., M. J. PERRY, AND K. L. CARDER. 1989. Modeling in situ phytoplankton absorption from total absorption spectra in productive inland marine waters. *Limnol. Oceanogr.* **34**: 1510–1523.
- SMITH, R. C., AND K. S. BAKER. 1981. Optical properties of the clearest natural waters (200–800 nm). *Appl. Opt.* **20**: 177–184.
- SOGANDARES, F. M., AND E. S. FRY. 1997. Absorption spectrum (340–640 nm) of pure water. I. Photothermal measurements. *Appl. Opt.* **36**: 8699–8709.
- SOKOLIK, I., A. ANDRONOVA, AND T. C. JOHNSON. 1993. Complex refractive index of atmospheric dust aerosols. *Atmos. Environ.* **27**: 2495–2502.
- SOKOLIK, I. N., AND O. B. TOON. 1999. Incorporation of mineralogical composition into models of the radiative properties of mineral aerosol from UV to IR wavelengths. *J. Geophys. Res.* **104**: 9423–9444.
- STRAMSKI, D. 1999. Refractive index of planktonic cells as a measure of cellular carbon and chlorophyll *a* content. *Deep-Sea Res. I* **46**: 335–351.
- , E. BOSS, D. BOGUCKI, AND K. J. VOSS. 2004a. The role of seawater constituents in light backscattering in the ocean. *Prog. Oceanogr.* **61**: 27–56.
- , A. BRICAUD, AND A. MOREL. 2001. Modeling the inherent optical properties of the ocean based on the detailed composition of the planktonic community. *Appl. Opt.* **40**: 2929–2945.
- , AND C. D. MOBLEY. 1997. Effects of microbial particles on oceanic optics: A database of single-particle optical properties. *Limnol. Oceanogr.* **42**: 538–549.
- , AND J. PISKOZUB. 2003. Estimation of scattering error in spectrophotometric measurements of light absorption by aquatic particles from three-dimensional radiative transfer simulations. *Appl. Opt.* **42**: 3634–3646.
- , AND S. B. WOŹNIAK. 2005. On the role of colloidal particles in light scattering in the ocean. *Limnol. Oceanogr.* **50**: 1581–1591.

- , ———, AND P. J. FLATAU. 2004*b*. Optical properties of Asian mineral dust suspended in seawater. *Limnol. Oceanogr.* **49**: 749–755.
- TASSAN, S., AND G. M. FERRARI. 2003. Variability of light absorption by aquatic particles in the near-infrared spectral region. *Appl. Opt.* **42**: 4802–4810.
- TORRENT, J., U. SCHWERTMANN, H. FECHTER, AND F. ALFEREZ. 1983. Quantitative relationships between soil color and hematite content. *Soil Sci.* **136**: 354–358.
- WOŹNIAK, B., S. B. WOŹNIAK, K. TYSZKA, M. OSTROWSKA, R. MAJCHROWSKI, D. FICEK, AND J. DERA. 2005. Modelling the light absorption properties of particulate matter forming organic particles suspended in seawater. Part 2. Modelling results. *Oceanologia* **47**: 621–662.
- WOŹNIAK, S. B., AND D. STRAMSKI. 2004. Modeling the optical properties of mineral particles suspended in seawater and their influence on ocean reflectance and chlorophyll estimation from remote sensing algorithms. *Appl. Opt.* **43**: 3489–3503.
- ZANEVELD, J. R. V., J. KITCHEN, AND C. MOORE. 1994. The scattering error correction of reflecting-tube absorption meters, p. 44–55. *In* J. S. Jaffe [ed.], *Ocean optics XII*, Proc. SPIE **2258**.

Received: 29 November 2006

Accepted: 7 June 2007

Amended: 13 June 2007